IEEE Access
Multidisciplinary | Rapid Review | Open Access Journal

Received April 30, 2018, accepted June 2, 2018, date of publication June 13, 2018, date of current version June 29, 2018.

Digital Object Identifier 10.1109/ACCESS.2018.2846728

Optimized Optical Coherence Tomography Imaging With Hough Transform-Based Fixed-Pattern Noise Reduction

YINGWEI FAN[1], LONGFEI MA[1], WEI CHANG[1], WEIPENG JIANG[1], SITE LUO[2], XINRAN ZHANG[1], AND HONGEN LIAO[1], (Senior Member, IEEE)

[1]Department of Biomedical Engineering, School of Medicine, Tsinghua University, Beijing 10084, China
[2]Department of Electronic Engineering, Tsinghua University, Beijing 10084, China

Corresponding author: Hongen Liao (liao@tsinghua.edu.cn)

This work was supported in part by the Beijing Municipal Science & Technology Commission under Grant Z151100003915079, in part by the Beijing Municipal Natural Science Foundation under Grant 7172122 and Grant L172003, in part by the National Key Research and Development Program of China under Grant 2017YFC0108000, and in part by the National Natural Science Foundation of China under Grant 81427803 and Grant 81771940.

ABSTRACT Fixed-pattern noise seriously affects the clinical application of optical coherence tomography (OCT), especially, in the imaging of tumorous tissue. We propose a Hough transform-based fixed-pattern noise reduction (HTFPNR) method to reduce the fixed-pattern noise for optimizing imaging of tumorous tissue with OCT system. Using by the HTFPNR method, we detect and map the outline of fixed-pattern noise in the OCT images, and finally efficiently reduce the fixed-pattern noise by the longitudinal and horizontal intelligent processing procedure. We adopt the image-to-noise ratio with full information (INR_{fi}) and the noise reduction ratio (NRR) to evaluate the outcome of fixed-pattern noise reduction ratio, respectively. The INR_{fi} of OCT image's noise reduction of *ex vivo* brainstem tumor is approximate 21.92 dB. Six groups of OCT images, including three types of fixed-pattern noises, have been validated via experimental evaluation of the *ex vivo* gastric tumor. In the different types of fixed-pattern noise, the mean INR_{fi}s are 25.24, 23.04, and 19.35 dB, respectively. This result demonstrates that it is highly efficient and useful in fixed-pattern noise reduction. The fluctuating range of the NRR is 0.84–0.88 for three types of added noise in the OCT images. This result demonstrates that the HTFPNR method can as possible as save useful information by comparing to previous research. This proposed HTFPNR method can be used into the fixed-pattern noise reduction of OCT images in other soft biological tissue in the future.

INDEX TERMS Optical coherence tomography, fixed-pattern noise reduction, Hough transform, tumor imaging.

I. INTRODUCTION

Optical coherence tomography (OCT) is a noninvasive, and label-free imaging technique for the image acquisition of the cross-sectional semi-transparent biological tissue [1]. OCT can provide the millimeter-size deep [2]–[4]. Imaging quality is limited by the biological-tissue scattering, which decreases with the increase of the light's wavelength [5]–[8]. The high image quality of an OCT system is important to help realize the real-time identification of diseased tissue in the integration of diagnosis and therapeutic [9]–[12]. Recently, some researchers focus on the novel system construction [13], coherence signal processing, and image processing to improve the readability of OCT images [14]. Fixed-pattern noise [15] will directly influence the identification of tumorous or cancerous tissue in the OCT images, so that there are misjudgments in the diagnosis of conventional surgical guidance or novel theranostics. Hence, the fixed-pattern noise reduction is significant for the assisting the surgeons to implement the precision identification of the tumorous tissue.

Fixed-pattern noise of the OCT image in horizontal and longitudinal orientation results from the abrasion of an OCT system's component and the strong reflection on the surface of biological tissue, respectively. In the longitudinal orientation, it is also called as central artefact [16]. Methods of subtracting the ensemble average of spectra and a naïve Bayes mask-based binary mask have been developed to eliminate the autocorrelation artefacts and background noise reduction, respectively [17], [18]. OCT image is acquired through subtracting mean value of the background image in the lines of

an OCT system [19], this method of background noise reduction improves the quality of coherence and cross-sectional images. Furthermore, other methods have been proposed through the ways to improve the performance of the hardware and software for the removal of the fixed-pattern noise. On the hardware side, the balance detection method [20] and the graphic processing unit (GPU) assisted partial median subtraction method [21] also can efficiently reduce the fixed-pattern noise. However, these methods increase the system cost and additional power. On the software side, spectral reduction-based methods [22], [23] also can remove the fixed-pattern noise. The histogram-based denoising algorithm [24] and an aligning interferogram method [25] can reduce the fixed-pattern noise. However, these methods remove the useful information to some extent. Most of above methods have the same characteristics, which are only suitable to reduce horizontal fixed-pattern noise. Fixed-pattern noise intuitively simulates a quasi-straight line. The Hough transform-based noise reduction algorithms have been developed to segment special tissue in OCT image [16], [26]. Hough transform [27]–[32] is usually used to detect a straight line [33]–[35]. Hence, we point that the useful tool for detecting the straight lines or quasi-lines in tumorous tissue OCT images includes Hough transform and intelligent processing method, which can remove fixed-pattern noise effectively.

In this study, to remove fixed-pattern noise, we propose a practical Hough transform-based fixed-pattern noise reduction (HTFPNR) method, which can detect and remove the horizontal and longitudinal fixed-pattern noise of OCT images of a tumorous tissue, and the useful information can be saved completely for tumor imaging. This approach does not increase hardware costs of Fourier domain OCT (FD-OCT) system. The proposed method is applied into a FD-OCT system with high fixed-pattern noise suppression. The evaluation experiment of the noise suppression has been conducted about OCT images of the *ex vivo* brainstem and gastric tumor, and the evaluation index NRR and $\mathrm{INR_{fi}}$is computed to demonstrate the results of fixed-pattern noise reduction.

II. METHODS

The raw signal, which is the light intensity spitted by a spectrometer, is obtained by the linear charge-coupled device (CCD). An acquired line signal includes the interference signal between reference and sample arm; it can be expressed as Eq. (1) [36]:

$$\mathrm{I}(k) = (TR)|s(k)|^2\{R_r + \sum_i R_i + \sum_{i\neq j}\sqrt{R_iR_j}\cos[k(h_i - h_j)] + 2\sum_i \sqrt{R_iR_j}\cos(kh_i)\} \quad (1)$$

where T and R represent power transmissivity and the reflectivity of a beam splitter, respectively; k is the wave number; $s(k)$ is the light source spectral intensity; R_r is the reflectivity of the reference arm; R_i, R_j is the reflectivity of the sample arm; and h_i, h_j is the localization of different sample depth. Eq. 1 can be used to transform signal into a mapping relationship between wavenumber domain and optical-path difference domain. The acquired coherence signal is a function of wavelength domain. Furthermore, the relationship between wavenumber k and wavelength λ can be expressed as $k = \frac{2\pi}{\lambda}$. To reconstruct B-scan OCT image, the inverse fast Fourier transform (iFFT) of the interpolated wavenumber-domain interference signal demonstrates that depth profile reaches micrometer level.

A. BACKGROUND NOISE REDUCTION USING TWO-STEP FILTERING METHOD

Our aim is to subtract background noise from an OCT coherence signal and/or image. We propose a two-step filtering method for background noise reduction before the reconstruction of OCT image. The first step is to acquire the signal reference arm through the raw interference signal. The second step is to apply a median filter to process the coherence signal by treating the mirror as a sample. Furthermore, we acquire the filtered signal, which excluded the background component. The length of the median filter affected the result of the processed signal. Therefore, we choose better results with respect to the length of median filter.

We process the interpolative data by adding the *Taylor* window and applying the iFFT in the interference signal to acquire the sample's depth-resolved profile, which is the image function. The function can be expressed as Eq. (2):

$$\mathrm{i}(h) = \mathrm{FT}^{-1}[I(k)] = \frac{1}{2\pi} \times \int_{-\infty}^{+\infty} [I(k) - I_{ref}(k)] \times window \times \exp[j(kh)]dk \quad (2)$$

Where $I(k)$ is the intensity of the interference signal, $I_{ref}(k)$ is the light intensity of the reference arm, and the window is chosen as the *Taylor* window. This processing flow chart is same as the part of the direct component and background noise reduction (Fig. 1). The OCT image is reconstructed post background noise reduction.

B. HORIZONTAL MEAN REMOVAL-BASED PREPROCESSING METHOD IN TUMOROUS TISSUE'S OCT IMAGE

For preprocessing the OCT image of *ex vivo* tumor specimens, we conduct a horizontal mean-based noise removal method to reduce the partial fixed-pattern noise of OCT images. The acquired M-by-N OCT image I can provide the huge convenience for the post-processing. This procedure of noise reduction is as follows (Fig. 2).

Firstly, the preprocessing of the OCT image. Normalize the matrix I into 0-255.

Secondly, computing of the means of the lines. Compute the longitudinal orientation (M-orientation) mean value $\vec{M}$ in the image with the fixed-pattern noise I.

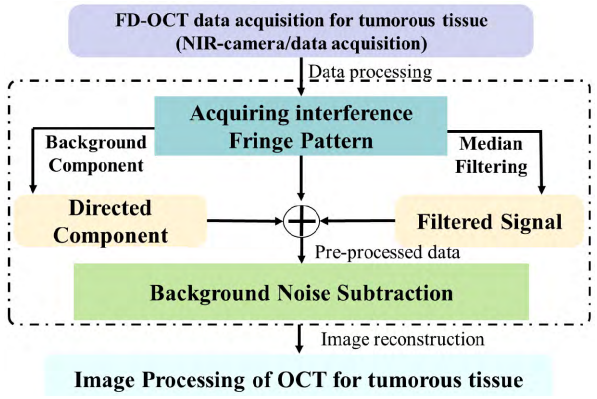

FIGURE 1. The flow diagram of a two-step filtering method for background noise.

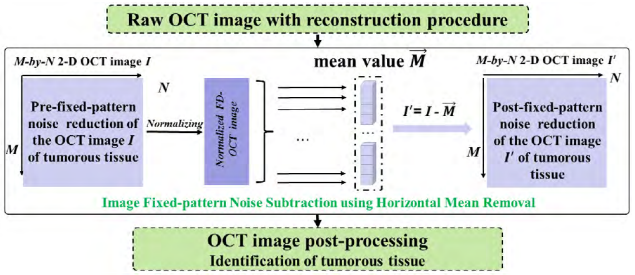

FIGURE 2. The process flowchart of horizontal mean removal-based noise reduction.

Thirdly, reducing the fixed-pattern noise preliminarily. Subtract the mean value $\overrightarrow{M}$ in accordance with the line of matrix I (M-orientation). The output matrix $I^{'}$ is the OCT image with the fixed-pattern noise reduction.

The image will afford feasible access to enhance the fixed-pattern noise reduction to the following processing. The output OCT images can afford the original effects on fixed-pattern noise reduction with the horizontal mean-based noise removal.

C. FIXED-PATTERN NOISE REDUCTION WITH HTFPNR METHOD IN TUMOROUS TISSUE'S OCT IMAGE

In order to increase the attenuation of different types of fixed-pattern noise, a HTFPNR method has been proposed for the OCT imaging of tumorous tissue post horizontal mean removal. The flowchart of the HTFPNR method is as shown as in Fig. 3. The method is based on the Hough transform algorithm, which detects the Hough lines and searches points around the Hough lines, to detect the lines and points in OCT images of *ex vivo* brainstem and gastric tumor. The fixed-pattern noise has some different types as shown in Fig. 3 (pointed by the green arrows). All images are processed in MATLAB. The Hough transform is implemented by the function *hough*, *houghpeaks* and *houghlines*. The function *hough* implements the Standard Hough Transform. Edge detection uses the function *edge*. *Canny* operator is used into detecting the image edge. The detailed processing procedure is described as following steps:

Step 1. Input raw OCT images of the tumorous tissue and initialize the parameters and pre-processing (translate the RGB images to gray images).

Step 2. Perform the Hough transform to gray images: acquire two points of every line (start-points and end-points) and the rotation angle |*theta*| of every Hough line; and use the two points to get the Hough line equation.

Step 3. Utilize the rotation angle |*theta*| to judge the lines whether horizontal or longitudinal lines (|*theta*| is approximately equal to 0 or 90 degree, respectively). *thre*1 and *thre*2 are the thresholds of the rotation angle of the lines. If |*theta*| is less than *thre*1, the line is treated as horizontal fixed-pattern noise; If |*theta*| is more than *thre*2, the line is treated as longitudinal fixed-pattern noise.

Step 4. Compute the distance between every pixel and the Hough lines in OCT image to find the point around the Hough lines.

Step 5. If the line is horizontal, we find the distance is not lower than threshold n, and let the grayscale of these pixels equal to *zero*. If the line is longitudinal, we find the distance is not lower than threshold n, and interpolate the grayscale of these pixels with the nearest points.

Step 6. Search the upper boundary of the tumorous tissue in OCT images (the image above the boundary of the tumorous tissue has nothing), therefore, let the grayscale of these pixels equal to *zero*.

Step 7. Compute the evaluation index of fixed-pattern noise reduction, which is measured by $\mathrm{INR_{fi}}$ (Eq. (3)), the index will give the quantitative evaluation effect of the fixed-pattern noise reduction of the tumorous tissue's OCT images.

Step 8. End the processing and output the OCT images without the fixed-pattern noise.

D. EVALUATION OF THE NOISE REDUCTION RATIO

In order to evaluate the noise reduction, we conduct the noise reduction ratio (NRR) to compute the noise reduction index of OCT images, which include the added noise that is reduced by the HTFPNR method. The NRR is defined to demonstrate the performance of our algorithm, as Eq.(3):

$$\mathrm{NRR} = \frac{10\log_{10}(\sum I^2_{noise\_filtered})}{10\log_{10}(\sum I^2_{add\_noise})} \tag{3}$$

where $I_{noise\_filtered}$ and I_{add_noise} are the intensities of the added noise and noise removed using the algorithm, respectively. Moreover, we use the $\mathrm{INR_{fi}}$ to validate the fixed-pattern noise reduction for OCT images of *ex vivo* tumor specimens. The $\mathrm{INR_{fi}}$ gives the power ratio between OCT image and its fixed-pattern noise for the biological tissue. The $\mathrm{INR_{fi}}$ can be defined as Eq. (4):

$$\mathrm{INR_{fi}}[dB] = 20 \times \log_{10}\left(\frac{\sqrt{\frac{1}{N}\sum I^2_{filtered}}}{\sqrt{\frac{1}{N}\sum I^2_{noise}}}\right) \tag{4}$$

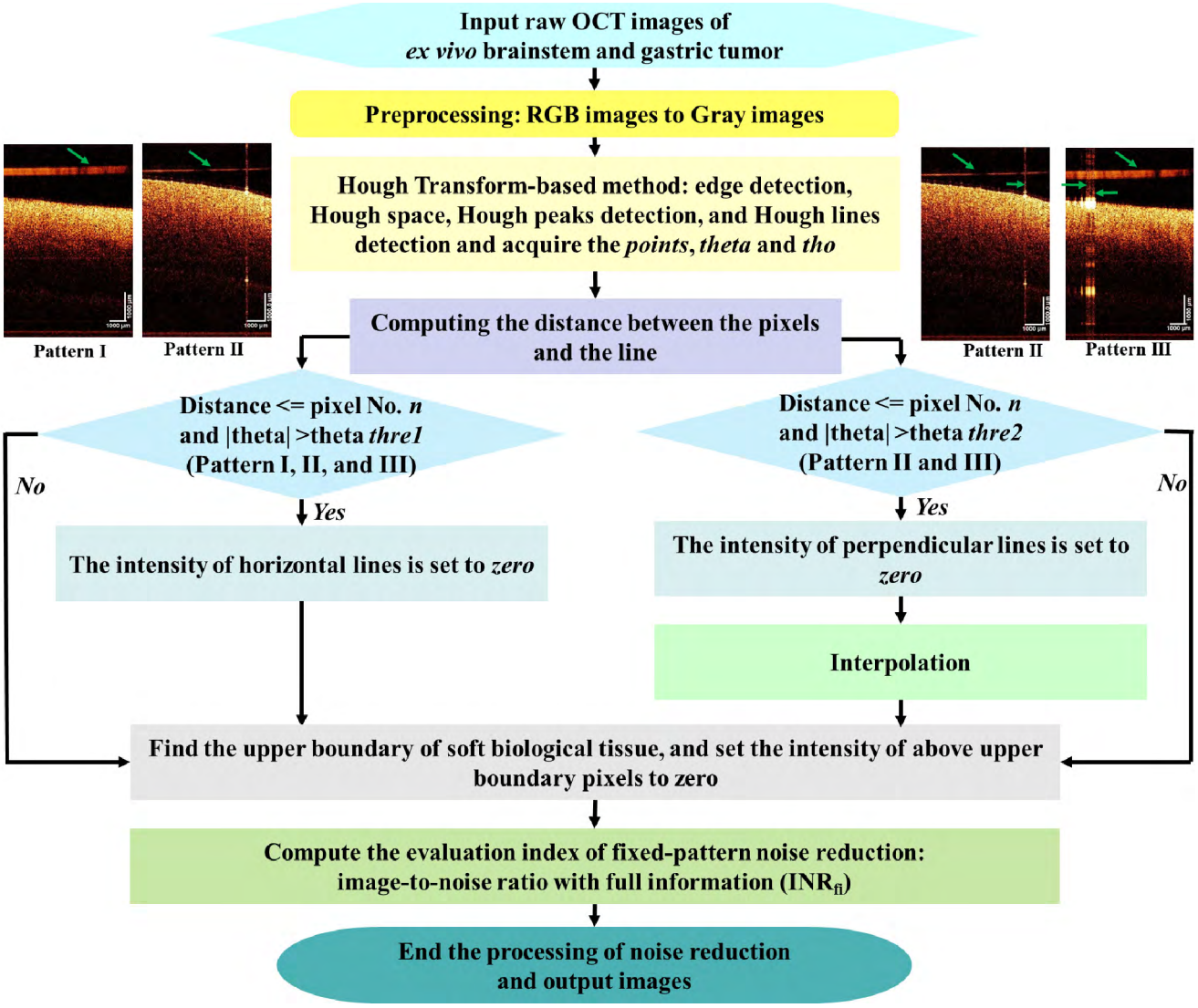

FIGURE 3. The flowchart of using the HTFPNR method of OCT images. The fixed-pattern noise has three types: artefact pattern I, artefact pattern II and artefact pattern III. Pattern I includes full horizontal noise, Pattern II includes full horizontal noise and one longitudinal quasi-line fixed-pattern noise, Pattern III includes full horizontal noise and two or more longitudinal quasi-lines.

where N is the total number of pixels, and $I_{filtered}$ is the image intensity without the fixed-pattern noise, I_{noise} is the noisy image intesinty.

The *ex vivo* brainstem tumor and gastric tumor has been imaged and analyzed. We compute and contrast the INR_{fi} of different types of the fixed-pattern noise in our OCT images of *ex vivo* brainstem and gastric tumors. There are three types of the artefact: artefact pattern I, artefact pattern II and artefact pattern III in OCT images of *ex vivo* gastric tumor. Pattern I has only horizontal fixed-pattern noise, Pattern II has horizontal and single longitudinal fixed-pattern noise, and Pattern III has horizontal and multiple longitudinal fixed-pattern noise. These types of the fixed-pattern noises are as shown in Fig 3 (pointed by green arrows in the OCT images). The OCT images on the left show the artefact pattern I and artefact pattern II, and the green arrows point to the horizontal fixed-pattern noise. The OCT images on the right show the artefact pattern II and artefact pattern III, the green arrows point to the longitudinal fixed-pattern noise. They include most types of fixed-pattern noises in our OCT images. Therefore, we analyze the differences of these types of INR_{fi} and summarize the effects of the fixed-pattern noise reduction with the HTFPNR methods with the OCT images of the *ex vivo* brainstem and gastric tumors.

III. EXPERIMENTS AND RESULTS

For the purpose of producing a spectral signal and acquiring an interference signal, we designed an OCT system to scan the tumorous tissue. This OCT system is as shown in Fig. 4 (a)). The central wavelength and bandwidth of the temporal coherence light source determine the longitudinal

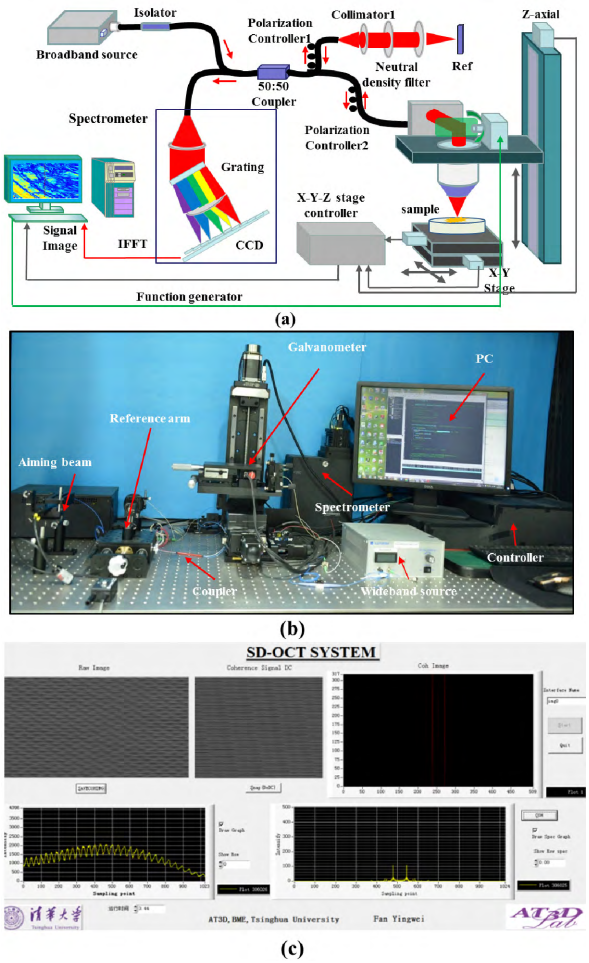

FIGURE 4. (a) The configuration of Fourier domain OCT system; (b) The physical setup of Fourier domain OCT system; (c) The user interface of FD-OCT system.

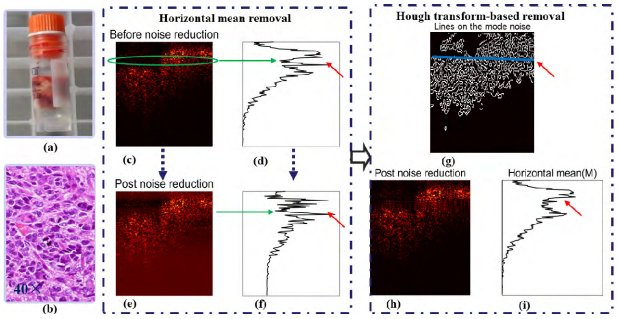

FIGURE 5. (a) and (b) the brainstem tumor specimen and its pathological resection; (c)-(f) the procedure and results of fixed-pattern noise reduction based on horizontal mean removal method (in the first blue dashed box); (c) and (e) the OCT image before and after fixed-pattern noise reduction based on horizontal mean removal method; (d) and (f) the horizontal mean corresponding to (c) and (e), the red arrow shows the fixed-pattern noise; (g)-(i) the results of fixed-pattern noise reduction based on Hough transform method (in the second blue dashed box); (g) the Hough line with different colors in edge-detection image; (h) the denoised OCT image with the HTFPNR method; (i) the horizontal mean corresponding to (h).

resolution of OCT, and its spatial coherence has an important influence on lateral and longitudinal resolution.

The light of a near-infrared broadband source is coupled with optical fiber; the source has the central wavelength of 1310 nm and full-width at half maximum bandwidth of 82 nm, respectively, at maximum drive current (Miunilite series, Bayspec, California, USA). The engine had an integrated Volume Phase Grating spectrograph (DeepView OCT Shortwave-infrared Series, Bayspec, California, USA), and the linescan camera had an InGaAs detector (SU1024LDM, GOODRICH, North Carolina, USA) with high sensitivity to near-infrared light. Coherence signal is detected by the spectrometer and infrared camera. The fiber coupler includes the single mode fiber (TW1300R5A2, THORLABS, New Jersey, USA), whose bandwidth was approximately 100 nm and center wavelength was 1310 nm. Furthermore, a two-dimensional image (B-scan) can be captured by the scanning of the one-dimension galvanometer mirror scanner (GVS001, THORLABS, New Jersey, USA). Subsequently, the signal is digitized by an image acquisition card (NI-IMAQ PCIe-1427, National Instruments, Texas, USA). The depth-resolved profile (A-line) is obtained by the IMAQ through converting the interference signal detected into linear k-space. The sample arm has an electrical-controlling moving platform. This platform conveys tumorous tissues, such as brainstem and gastric tumors. It can be adjusted to appropriate light path difference to acquire more high-definition OCT images.

User interface of the OCT system is designed and setup with *LabWindows/CVI* (2013, National Instruments, Texas, USA). It is used as a tool for signal processing, image acquisition and storage. The user interface displays the raw coherence signal, its iFFT and tomographic image of biological tissue. The physical setup of the OCT system is as shown in Fig. 4 (b). According to the scanning method of galvanometer mirror, the speed frequency of scanning could be set to 0.25 Hz, and it depends on the speed of the image acquisition. The theoretical axial and longitudinal resolutions of the OCT system are approximately 10.0 μm and 9.2 μm, respectively.

A. RESULTS OF BACKGROUND NOISE REDUCTION OF COHERENCE SIGNAL

We applied the algorithm of background noise reduction in interference signal processing. Simultaneously, the directed component of coherence signal decreased through performing this method. Before the processing, the depth-resolved profile demonstrated that the directed component remained significantly. After removing the background noise, the signal was processed by the median-filtering method and the *Taylor* window function was added.

We demonstrated the iFFT results of a raw interference signal through background noise subtraction. The light intensity of the reference arm was obtained by the OCT system through keeping the light out of the sample arm. Then, we subtracted the reference arm light intensity from the interference signal to reduce the background noise. We obtained the best result using the median filtering width of 40 sampling points after

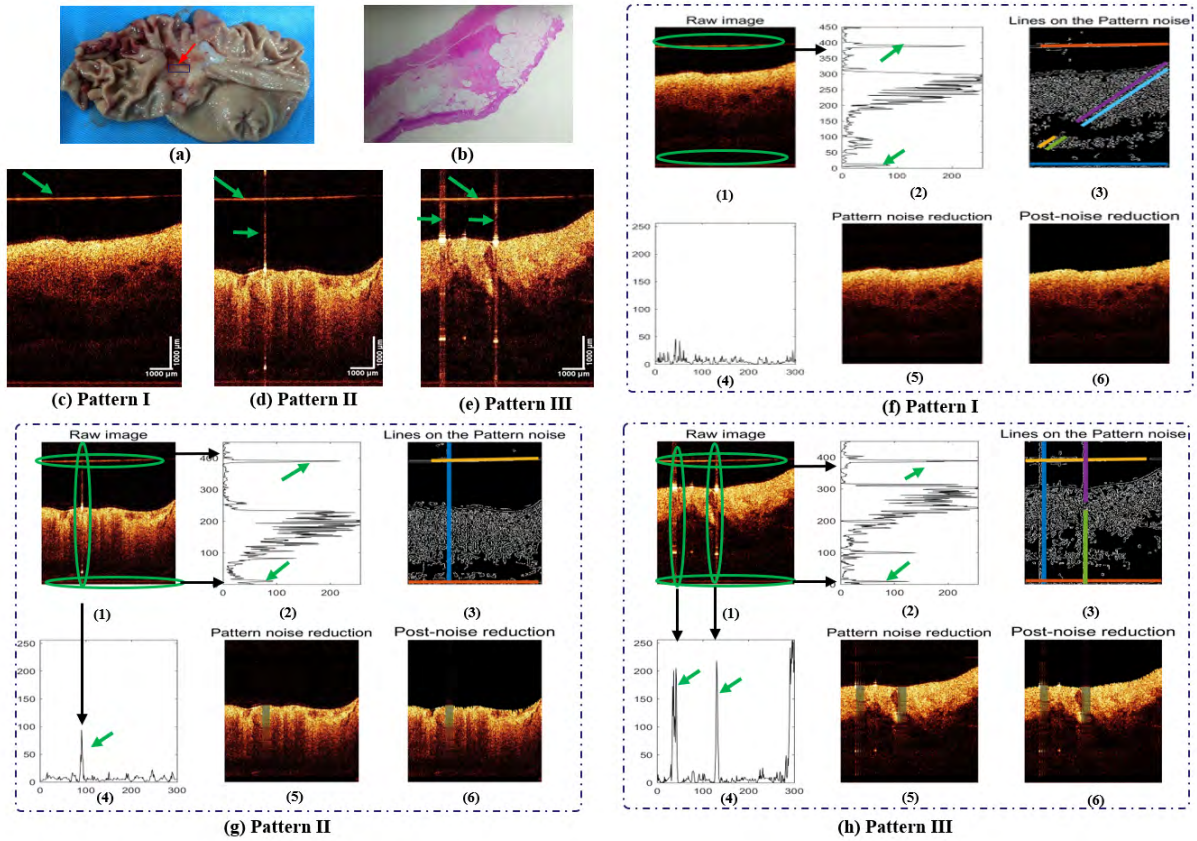

FIGURE 6. The validation experiment of fixed-pattern noise reduction of *ex vivo* gastric cancer imaging with HTFPNR method. (a) and (b) The *ex vivo* gastric cancer specimens and its histopathological section; (c), (d) and (e) the raw OCT images (acquired in the location of gastric cancer (a) with green arrow, fixed-pattern noise has three types: artefact pattern I, artefact pattern II and artefact pattern III); (f), (g) and (h), subfigure (1) the locations of fixed-pattern noise with green ellipses, subfigures (2) and (4) the signal located in (1) with blue lines, subfigure (3) the Hough lines with different colors in the edge-detection image, subfigure (5) the OCT images without Hough lines, subfigure (6) the OCT images without fixed-pattern noise (removal the noise on the upper surface).

several attempts. Finally, the attenuation of directed component reached up to 6.14 dB.

B. RESULTS OF THE HTFPNR METHOD OF EX VIVO BRAINSTEM TUMOR OCT IMAGES

The imaging experiments of the brainstem tumor specimen were conducted. Experimental *ex vivo* brainstem tumorous specimens were obtained during neurosurgery for the tumor resection and immediately put into frozen pipes (Fig. 5(a)); the frozen pipes were then put in liquid nitrogen. The resection was imaged by our OCT system.

Following the analysis, the brainstem tumorous specimens were 4.5% formalin fixed and were embedded with paraffin for standard histological analysis and processing: which includes fixing, dehydrating, paraffin inclusion *etc*. Histological sections were evaluated by pathologists. Here, the size of brainstem tumor was not enough to support the scanning of the OCT imaging. We just chose the appropriate size of OCT image for utilizing the effective information.

We acquired OCT images of the brainstem tumor specimen and horizontal mean of OCT image (Figs. 5(c) and (d), respectively). The effect of horizontal mean removal is as shown in Fig. 5(e), and its horizontal mean is as shown in Fig. 5(f). In these subfigures, the red arrow points to fixed-pattern noise. The HTFPNR method is used to process the OCT image. Figs. 5(g)-(h) demonstrate the results of fixed-pattern noise reduction for OCT images of brainstem tumor. (g) is the detected Hough line in the edge-detection image, which overlaps to the fixed-pattern noise; (h) is the OCT image after the processing of HTFPNR method to reduce fixed-pattern noise; (i) is the horizontal mean corresponding to (h). The INR_{fi} reached about 21.92 dB. In the subfigures (d) and (i), we can get the effect of fixed-pattern noise reduction (as the red arrow pointing to), the attenuation of fixed-pattern noise is significant.

C. VALIDATION EXPERIMENTAL RESULTS OF THE HTFPNR METHOD OF EX VIVO GASTRIC TUMOR'S OCT IMAGES

Experimental OCT images of the *ex vivo* gastric cancer were obtained during the neurosurgical procedures for surgical tumor resection from operating room (Fig. 6(a)). To validate the method, the resected specimen was imaged by another FD-OCT system. The FD-OCT system has same features of the *ex vivo* specimens of tumorous tissue. The imaged

position was where the red arrow points to (Fig. 6(a)), and it is the boundary between normal tissue and tumorous tissue of the gastric tumor specimens through experienced surgeon's identification. Due to current standard procedure of histological section is separated and complicated. Therefore, the observation location was not absolutely match to histological section. The observation location of histological section was as much as possibly close to the imaging location with the FD-OCT system by labeling the feature points. The specimens were 4.5% formalin fixed and were embedded with paraffin for standard histological analysis. Histological sections were evaluated by pathologists (Fig. 6(b)).

We acquired OCT image of *ex vivo* gastric cancerous specimen (Figs. 6(c), (d) and (e)). The OCT images had pixels of 450×300, and the size of OCT image was approximately 15 mm × 5 mm. The fixed-pattern noise has three types: artefact pattern I, artefact pattern II and artefact pattern III as previous described. The validation of the fixed-pattern noise reduction with HTFPNR method is as shown in subfigure (6) in the Figs. 6(f), (g) and (h). The effect of fixed-pattern noise reduction was significant and high efficient. A noteworthy tomographic structure of cancerous tissue is as displayed in Fig. 6(d) and (e). Furthermore, fixed-pattern noise reduction of three types has been displayed subfigures (1)-(6) in the Figs. 6 (f), (g) and (h). The high-quality OCT (subfigure (6) in the Figs. 6(f), (g) and (h)), which has reduced the fixed-pattern noise in the perpendicular and horizontal orientation, can give us denoised visual view to analyze the cross-sectional OCT images.

D. VALIDATION EXPERIMENTAL RESULTS OF THE HTFPNR METHOD OF EX VIVO GASTRIC TUMOR'S OCT IMAGES WITH SIMULATED FIXED-PATTERN NOISE

For validation of the different types of fixed-pattern noise reduction, we calculated the INR_{fi} of the denoised OCT images with these three types. Six groups of the INR_{fi}s about OCT images had been given about the *ex vivo* gastric tumor. The INR_{fi} of OCT images with the fixed-pattern noise reduction is approximately 22.00 dB (Fig. 7(a)). As the intensity of different types of the fixed-pattern noise increases, the INR_{fi}s have a downward trend, and this trend accords with the rule of noise reduction. We also get the means and variances of the INR_{fi}s with regard to six groups of OCT images. The means of INR_{fi} are 25.24 dB, 23.04 dB and 19.35 dB, and the standard deviations of the INR_{fi} are 5.94 dB, 10.61 dB and 2.57 dB (Fig. 7(b)). The means of INR_{fi} have same characteristics (Fig. 7(a)), it demonstrates that the HTFPNR method has different effects with the different types of fixed-pattern noise. The INR_{fi}s show that there is high-SNR noise reduction in the OCT images of the tumorous tissue.

For evaluate the reduction of three types of fixed-pattern noise, we added the simulated fixed-pattern noise with arbitrary power value P_{mn} (50, 60, 70, 80, 90, 100 dB) to the denoising OCT image of the *ex vivo* gastric tumor. These OCT images with added noise is as shown in subfigure (1) in the Figs. 8 (a, b, c). The detected lines with different colors are

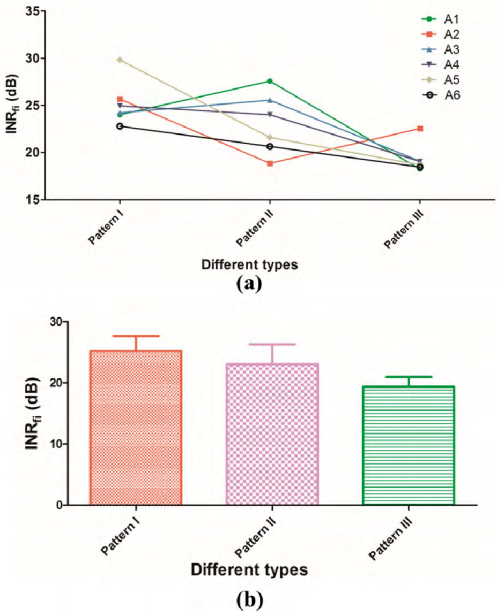

FIGURE 7. (a) The INR_{fi}s of six groups of OCT images with three types fixed-pattern noise; (b) the means and standard deviations of the INR_{fi} of three types of OCT images with fixed-pattern noise.

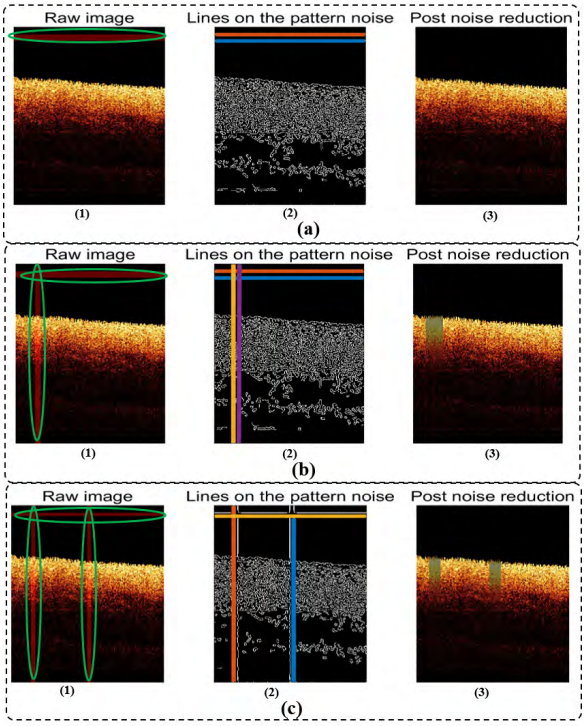

FIGURE 8. The OCT images with simulated noise (Pattern I, II and III) and OCT images with fixed-pattern noise reduction with the HTFPNR method. (1) The locations of fixed-pattern noise with green ellipses, (2) the Hough lines with different colors in edge-detection image, (3) the OCT images without fixed-pattern noise (removal the noise on the upper surface). (a) Simulated Pattern I. (b) Simulated Pattern II. (c) Simulated Pattern III.

shown in subfigure (2) in the Figs. 8 (a, b, c), corresponding to Pattern I, II, III, respectively. The NRRs were computed and they reached the minimum value of 0.84 and the maximum

TABLE 1. The NRRs of the proposed method through adding the simulated fixed-pattern noise to OCT image.

Types	P_{mn}(dB)					
	50	60	70	80	90	100
Pattern I	0.84	0.84	0.85	0.85	0.86	0.85
Pattern II	0.86	0.87	0.87	0.87	0.88	0.87
Pattern III	0.86	0.86	0.86	0.86	0.87	0.87

TABLE 2. The NRRs of the proposed HTFPNR method and previous Histogram-based denoising method.

Methods	Min. NRR	Max. NRR
Histogram-based denoising algorithm[24]	0.87	1.16
The proposed HTFPNR method	0.84	0.88

value of 0.88 of three types of fixed-pattern noise (Table 1), respectively. Comparing to previous research [24] (Table 2), the NRRs of the proposed HTFPNR method is less than 1.00, generally. It demonstrates that the useful information is saved completely and fixed-pattern noise is as much as possibly reduced.

IV. DISCUSSION

A. CONTRIBUTIONS

We propose the HTFPNR method for fixed-pattern noise reduction of OCT images. This method can efficiently reduce different types of the fixed-pattern noise in the OCT image of the tumors. Results demonstrate the enhanced performance of direction component attenuation and the reliable outcomes with regard to fixed-pattern noise reduction. The HTFPNR method provides a new approach to reduce the fixed-pattern noise of the coherence signal and tomographic image in FD-OCT system for the imaging of the tumorous tissue, this method can optimize FD-OCT imaging and enhance the quality of OCT images for the clinical application.

B. ADVANCES

The background and fixed-pattern noise reduction method comprises the filtering and HTFPNR method, respectively. The method has different results with regard to the coherence signal and fixed-pattern noise reduction. In our experiment, a median filtering showed that the attenuation coefficient reaches up to the high value. We find that the attenuation and suppression effect of the directed component is very significant; therefore, the useful information is enhanced to help to analyze and identify the tumorous tissue. Fixed-pattern noise without overlapping useful information can be as possible as removed in the OCT images of *ex vivo* gastric tumor. Fixed-pattern noise has significant attenuation through the horizontal mean removal, while the useful information suffers some loss following noise reduction. To improve a removal effectiveness of non-useful information, we develop the HTFPNR method to detect the Hough lines in OCT images of the tumorous tissue. The NRR is always less than 1.00, it is demonstrated that this method can as much as possible remove fixed-pattern noise and completely save useful information; it has significant difference comparing to the histogram-based denoising algorithm [24]. Furthermore, it can be used into OCT image processing, especially in fixed-pattern noise reduction of biological tumorous tissue.

For the different types of a fixed-pattern noise in the OCT images of *ex vivo* gastric tumor, our method is very efficient for the Pattern I. This type shows that fixed-pattern noise has no overlapping with the useful information, and the fixed-pattern noise usually lies in horizontal orientation. Our method can completely remove the fixed-pattern noise for the Pattern I. For the types of Pattern II and Pattern III, fixed-pattern noise usually lies in longitudinal orientation and overlaps on the useful information. Fixed-pattern noise can be as much as possibly reduced, and it is replaced with neighboring information (the interpolation of grayscale) to reach best approximation. In the different types of fixed-pattern noise, the method has an effectiveness of noise suppression. In the Pattern II or III, the variance of INR_{fi}s has demonstrated the strong reflection on tumorous tissue surface can produce the high intensity of the fixed-pattern noise. Hence, we can set the appropriate situation to acquire high-quality OCT images based on appropriate situation. Furthermore, as previous described, the fixed-pattern noise has the feature of the quasi-line or straight line. We detect the Hough lines and reconstruct the fixed-pattern noises, then remove the noises. Similarly, our HTFPNR method also can be remove the noise, which has the feature of the quasi-line or straight line. This will be a wider range for more noise types to deal with in the future.

C. SOME LIMITATIONS

There are some further improved aspects of our HTFPNR method. Firstly, the evaluation approach of fixed-pattern noise reduction cannot be appropriately developed, and the effect of fixed-pattern noise reduction is simply judged intuitively. The high-quality OCT images will help us afford the real-time identification of the cancerous and non-cancerous tissue [6], [7]. Subsequently, in the longitudinal fixed-pattern noise reduction, the interpolation will result in unreal information and distortion in OCT image. A more reasonable interpolation method should be developed. In the horizontal fixed-pattern noise, the edge or surface of a soft biological tissue will be like a straight line in some cases, we will develop more reasonable method to reduce this impact. Lastly, the choice of a window function is based on noise-eliminating effect of a common window. We choose the *Taylor* window after multiple trials of different window functions and use it in our background noise suppression algorithm. To achieve better effects of the fixed-pattern noise suppression, the window function will be reselected according to the actual situation.

V. CONCLUSION

In summary, we propose a HTFPNR method to eliminate fixed-pattern noise of OCT images. This method has been

used into the OCT imaging for brainstem and gastric tumor. We conduct some evaluation experiments for validating the HTFPNR method. This method realizes the high-SNR effect on the three types of the fixed-pattern noise reduction. Results demonstrate the good performance of fixed-pattern noise reduction and the improvement of OCT image quality. The HTFPNR method will provide more intuitive-visual and high-quality imaging solutions for tumor imaging. Intraoperative *in vivo*, *in situ* OCT imaging and diagnosis for theranostics [9]–[12], [37], such as the integration of OCT and laser ablation system [9] of the tumorous tissue is an active and upcoming field of investigation, which will be applied to detect more microstructural information, especially, with regard to the real-time surgical guidance.

DISCLOSURES

The authors have declared that no competing interest exists.

ACKNOWLEDGMENT

We thank Prof. Liwei Zhang and Dr. Jie Tang with Beijing Tiantan Hospital, Capital Medical University, Beijing, China for providing brainstem tumor specimens and clinical assistance.

REFERENCES

[1] D. Huang *et al.*, "Optical coherence tomography," *Science*, vol. 254, no. 5035, pp. 1178–1181, 1991.

[2] W. Drexler, M. Liu, A. Kumar, T. Kamali, A. Unterhuber, and R. A. Leitgeb, "Optical coherence tomography today: Speed, contrast, and multimodality," *J. Biomed. Opt.*, vol. 19, no. 7, p. 071412, 2014.

[3] E. A. Swanson and J. G. Fujimoto, "The ecosystem that powered the translation of OCT from fundamental research to clinical and commercial impact," *Biomed. Opt. Express*, vol. 8, no. 3, pp. 1638–1664, 2017.

[4] O. M. Carrasco-Zevallos *et al.*, "Review of intraoperative optical coherence tomography: Technology and applications," *Biomed. Opt. Express*, vol. 8, no. 3, pp. 1607–1637, 2017.

[5] S. L. Jacques, "Optical properties of biological tissues: A review," *Phys. Med. Biol.*, vol. 58, no. 11, pp. R37–R61, 2013.

[6] C. Kut *et al.*, "Detection of human brain cancer infiltration *ex vivo* and *in vivo* using quantitative optical coherence tomography," *Sci. Transl. Med.*, vol. 7, p. 292ra100, Jun. 2015.

[7] W. Yuan, C. Kut, W. Liang, and X. Li, "Robust and fast characterization of OCT-based optical attenuation using a novel frequency-domain algorithm for brain cancer detection," *Sci. Rep.*, vol. 7, Mar. 2017, Art. no. 44909.

[8] H.-C. Lee *et al.*, "Endoscopic optical coherence tomography angiography microvascular features associated with dysplasia in Barrett's esophagus (with video)," *Gastrointestinal Endosc.*, vol. 86, no. 3, pp. 476–484, 2017.

[9] Y. Fan, B. Zhang, W. Chang, X. Zhang, and H. Liao, "A novel integration of spectral-domain optical-coherence-tomography and laser-ablation system for precision treatment," *Int. J. Comput. Assist. Radiol. Surg.*, vol. 13, no. 3, pp. 411–423, 2018.

[10] Y. Fan *et al.*, "Optical coherence tomography for precision brain imaging, neurosurgical guidance and minimally invasive theranostics," *Biosci. Trends*, vol. 12, no. 1, pp. 12–23, 2018.

[11] H. Liao *et al.*, "Combination of intraoperative 5-aminolevulinic acid-induced fluorescence and 3-D MR imaging for guidance of robotic laser ablation for precision neurosurgery," in *Proc. 11th Int. Conf. Med. Image Comput. Comput.-Assist. Intervent.*, 2008, pp. 373–380.

[12] H. Liao *et al.*, "An integrated diagnosis and therapeutic system using intraoperative 5-aminolevulinic-acid-induced fluorescence guided robotic laser ablation for precision neurosurgery," *Med. Image Anal.*, vol. 16, no. 3, pp. 754–766, 2012.

[13] M. Siddiqui, A. S. Nam, S. Tozburun, N. Lippok, C. Blatter, and B. J. Vakoc, "High-speed optical coherence tomography by circular interferometric ranging," *Nature Photon.*, vol. 12, pp. 111–116, Feb. 2018.

[14] Y. Rao, H. Panakkal, N. Sarwade, and R. Makkar, "Signal and image processing of optical coherence tomography at 1310 nm wavelength for non biological samples," *Signal Image Process.*, vol. 6, no. 2, p. 53, 2015.

[15] J. F. de Boer, R. Leitgeb, and M. Wojtkowski, "Twenty-five years of optical coherence tomography: The paradigm shift in sensitivity and speed provided by Fourier domain OCT," *Biomed. Opt. Express*, vol. 8, no. 7, pp. 3248–3280, 2017.

[16] T. Zhang *et al.*, "A novel technique for robust and fast segmentation of corneal layer interfaces based on spectral-domain optical coherence tomography imaging," *IEEE Access*, vol. 5, pp. 10352–10363, 2017.

[17] R. K. Wang and Z. Ma, "A practical approach to eliminate autocorrelation artefacts for volume-rate spectral domain optical coherence tomography," *Phys. Med. Biol.*, vol. 51, no. 12, pp. 3231–3239, 2006.

[18] R. Reif, U. Baran, and R. K. Wang, "Motion artifact and background noise suppression on optical microangiography frames using a Naïve Bayes mask," *Appl. Opt.*, vol. 53, no. 19, pp. 4164–4171, 2014.

[19] B. C. Johnson, "Method and system for background subtraction in medical optical coherence tomography system," U.S. Patent 8 457 440 B1, Jun. 4, 2013.

[20] A. Bradu and A. G. Podoleanu, "Artifacts cancellation in Fourier domain optical coherence tomography using balance detection," in *Proc. SPIE*, vol. 8785, Porto, Portugal, 2013, p. 8785E4.

[21] Y. Watanabe, "Real time processing of Fourier domain optical coherence tomography with fixed-pattern noise removal by partial median subtraction using a graphics processing unit," *J. Biomed. Opt.*, vol. 17, no. 5, p. 050503, 2012.

[22] S. Moon, S. Lee, and Z. Chen, "Reference spectrum extraction and fixed-pattern noise removal in optical coherence tomography," *Opt. Express*, vol. 18, no. 24, pp. 24395–24404, 2010.

[23] J.-H. Kim, J.-H. Han, and J. Jeong, "Periodic reference subtraction method for efficient background fixed pattern noise removal in Fourier domain optical coherence tomography," *Opt. Commun.*, vol. 285, no. 7, pp. 2012–2016, 2012.

[24] K.-S. Kim, H.-J. Park, and H. S. Kang, "Enhanced optical coherence tomography imaging using a histogram-based denoising algorithm," *Opt. Eng.*, vol. 54, no. 11, p. 113110, 2015.

[25] G. Liu *et al.*, "Postprocessing algorithms to minimize fixed-pattern artifact and reduce trigger jitter in swept source optical coherence tomography," *Opt. Express*, vol. 23, no. 8, pp. 9824–9834, 2015.

[26] Z. Hubler, N. D. Shemonski, R. L. Shelton, G. L. Monroy, R. M. Nolan, and S. A. Boppart, "Real-time automated thickness measurement of the *in vivo* human tympanic membrane using optical coherence tomography," *Quant. Imag. Med. Surg.*, vol. 5, no. 1, pp. 69–77, 2015.

[27] P. Mukhopadhyay and B. B. Chaudhuri, "A survey of Hough transform" *Pattern Recognit.*, vol. 48, no. 3, pp. 993–1010, 2015.

[28] H.-Y. Chen, Y.-Y. Lin, and B.-Y. Chen, "Co-segmentation guided Hough transform for robust feature matching," *IEEE Trans. Pattern Anal. Mach. Intell.*, vol. 37, no. 12, pp. 2388–2401, Dec. 2015.

[29] Z. Xu, B. S. Shin, and R. Klette, "Accurate and robust line segment extraction using minimum entropy with Hough transform," *IEEE Trans. Image Process.*, vol. 24, no. 3, pp. 813–822, Mar. 2015.

[30] J. Zhang *et al.*, "3-D reconstruction of the spine from biplanar radiographs based on contour matching using the Hough transform," *IEEE Trans. Biomed. Eng.*, vol. 60, no. 7, pp. 1954–1964, Jul. 2013.

[31] N. Guil, J. Villalba, and E. L. Zapata, "A fast Hough transform for segment detection," *IEEE Trans. Image Process.*, vol. 4, no. 11, pp. 1541–1548, Nov. 1995.

[32] S. R. Deans, "Hough transform from the radon transform," *IEEE Trans. Pattern Anal. Mach. Intell.*, vol. PAMI-3, no. 2, pp. 185–188, Mar. 1981.

[33] C. Dalitz, T. Schramke, and M. Jeltsch, "Iterative Hough transform for line detection in 3D point clouds," *Image Process. On Line*, vol. 7, pp. 184–196, Jul. 2017.

[34] J. Guan, F. An, X. Zhang, L. Chen, and H. J. Mattausch, "Real-time straight-line detection for XGA-size videos by Hough transform with parallelized voting procedures," *Sensors*, vol. 7, no. 2, p. 270, 2017.

[35] W. Liu, Z. Zhang, S. Li, and D. Tao, "Road detection by using a generalized Hough transform," *Remote Sens.*, vol. 9, no. 6, p. 590, 2017.

[36] T. A. Alsaeed, M. Y. Shalaby, and D. A. Khalil, "Dispersion compensation in Fourier domain optical coherence tomography," *Appl. Opt.*, vol. 53, no. 29, pp. 6643–6653, 2014.

[37] H. Liao, "Integrated diagnostic and therapeutic techniques: Toward an intelligent medical system," *Comput. Med. Imag. Graph.*, vol. 38, no. 5, pp. 421–422, 2014.

YINGWEI FAN received the B.S. degree in biomedical engineering from the Kunming University of Science and Technology, Kunming, China, in 2012, and the master's degree in biomedical engineering from Northeastern University, Shenyang, China, in 2014. He is currently pursuing the Ph.D. degree with the Department of Biomedical Engineering, School of Medicine, Tsinghua University, Beijing, China.

His current research interests include minimally invasive theranostics, biomedical optics, medical image processing, and image-guided surgery.

LONGFEI MA received the B.S. degree in electronic information science and technology and the master's degree in underwater acoustic engineering from Harbin Engineering University, Harbin, China, in 2009 and 2012, respectively. He is currently pursuing the Ph.D. degree with the Department of Biomedical Engineering, School of Medicine, Tsinghua University, Beijing, China.

His current research interests include minimally invasive theranostics, biomedical optics, medical robotics, and image-guided surgery.

WEI CHANG received the B.S. degree in electrical engineering from the School of Electronic Information and Electrical Engineering, Shanghai Jiaotong University, Shanghai, China, in 2014. She is currently pursuing the master's degree with the Department of Biomedical Engineering, School of Medicine, Tsinghua University, Beijing, China.

Her current research interests include minimally invasive theranostics, biomedical optics, image processing, and deep learning.

WEIPENG JIANG received the B.S. and master's degrees from the School of Dentistry, Binzhou Medical University and Technology, in 2006 and 2010, respectively, and the Ph.D. degree from the School and Hospital of Stomatology, Peking University, in 2013. He holds a post-doctoral position with the Department of Biomedical Engineering, School of Medicine, Tsinghua University, Beijing, China.

His current research interests include minimally invasive theranostics, medical robotics, and image-guided surgery.

SITE LUO received the B.S. degree in mechanical engineering and the master's degree in mechanical engineering from Shandong University, Jinan, China, in 2010 and 2013, respectively. He is currently pursuing the Ph.D. degree with the Department of Electronic Engineering, Tsinghua University, Beijing, China.

His current research interests include optical coherence tomography, biomedical optics, and image-guided surgery.

XINRAN ZHANG received the B.S. degree in biomedical engineering from the South China University of Technology, Guangzhou, China, in 2013, and the master's degree from the Department of Biomedical Engineering, School of Medicine, Tsinghua University, Beijing, China, in 2016. She is currently a Research Associate with the Department of Biomedical Engineering, School of Medicine, Tsinghua University.

Her research interests include high quality and accuracy integral videography technologies and its application in 3-D surgical guidance system.

HONGEN LIAO (M'04–SM'14) received the B.S. degree in mechanics and engineering sciences from Peking University, Beijing, China, in 1996, and the M.E. and Ph.D. degrees in precision machinery engineering from the University of Tokyo, Tokyo, Japan, in 2000 and 2003, respectively. Since 2004, he has been a Faculty Member with the Graduate School of Engineering, University of Tokyo, where he became an Associate Professor in 2007. He has been selected as a National Thousand Talents Distinguished Professor, National Recruitment Program of Global Experts, China, since 2010. He is currently a Full Professor and the Vice Director of the Department of Biomedical Engineering, School of Medicine, Tsinghua University, Beijing. He was a Research Fellow of the Japan Society for the Promotion of Science.

He has authored or co-authored over 210 peer-reviewed articles and proceedings papers, 32 patents, over 290 abstracts, and numerous invited lectures. His research interests include 3-D medical image, image-guided surgery, medical robotics, computer-assisted surgery, and fusion of these techniques for minimally invasive precision diagnosis and therapy. He has also been involved in long viewing distance autostereoscopic display and 3-D visualization.

Dr. Liao was distinguished by receiving the government award [The Commendation for Science and Technology by the Minister of Education, Culture, Sports, Science and Technology (MEXT), Japan] and the National Eminent Expert of the National Recruitment Program of Global Experts, China. He received over ten awards including the IFMBE Young Investigators Awards in 2005 and 2006, respectively, the ERICSSON Young Scientist Award in 2006, the OGINO Award in 2007, and various Best Paper Awards from different academic societies. His research was well funded by MEXT, the Ministry of Internal Affairs and Communications, New Energy and Industrial Technology Development Organization, the Japan Society for the Promotion of Science in Japan, and the National Natural Science Foundation of China.

He is an Associate Editor of the IEEE Engineering in Medicine and Biology Society Conference, the Organization Chair of the Medical Imaging and Augmented Reality Conference (MIAR) 2008, the Program Chair of the Asian Conference on Computer-Aided Surgery Conference (ACCAS) 2008 and 2009, the Tutorial Co-Chair of the Medical Image Computing and Computer Assisted Intervention Conference (MICCAI) 2009, the Publicity Chair of MICCAI 2010, the General Chair of MIAR 2010 and ACCAS 2012, the Program Chair of MIAR 2013, the Workshop Chair of MICCAI 2013, and the General Co-Chair of MIAR 2016. He is a President of the Asian Society for Computer-Aided Surgery and Secretary of the Asian-Pacific Activities Working Group, International Federation for Medical and Biological Engineering.